ARTICLE

Influence of regioisomerism in bis(terpyridine) based exciplexes with delayed fluorescence

Received 00th January 20xx,
Accepted 00th January 20xx

DOI: 10.1039/x0xx00000x

A. Lennart Schleper,[a] Sabina Hillebrandt,[b,c] Christoph Bannwarth,[d] Andreas Mischok,[b] Seonil Kwon,[b] Florian Buchner,[e] Francisco Tenopala-Carmona,[b] R. Jürgen Behm,[e,f] Felix D. Goll,[a] Philipp J. Welscher,[a] Michael Usselmann,[a] Ulrich Ziener,*[a] Malte C. Gather,*[b,c] and Alexander J. C. Kuehne*[a,g]

Exciplexes of individual electron donor and acceptor molecules are a promising approach to utilizing otherwise non-emissive triplet states in optoelectronic applications. In this work, we synthesize a series of bis(terpyridine) pyrimidine (BTP) isomers and employ them as electron acceptors in complexes with tris(4-carbazoyl-9-ylphenyl)amine (TCTA). We show that these TCTA:BTP complexes produce thermally activated delayed fluorescence (TADF) by exciplex emission, and we investigate the influence of the nitrogen position in the pyridine on the optical and electronic properties of the exciplex. The molecular arrangement of the complex is studied using scanning tunneling microscopy (STM) and density functional theory (DFT) simulations. Finally, we fabricate organic light-emitting diodes (OLEDs) with maximum external quantum efficiencies ranging between 0.5% and 2% – depending on the BTP isomer.

Introduction

Thermally activated delayed fluorescence (TADF) has evolved as a powerful mechanism for the development of high-performance electroluminescent devices. TADF allows recycling of otherwise dark triplet states into emissive singlet states and internal quantum efficiencies of up to unity.[1–4] Most state-of-the-art TADF emitters contain covalently connected electron donor and acceptor units. By contrast, exciplexes form upon excitation of self-oriented complexes of individual donor and acceptor molecules. Typically, such donor acceptor complexes are created simply during co-deposition of organic hole- and electron transport materials.[5] Recently, organic light-emitting diodes (OLEDs) with exciplex emitters consisting of tris(4-carbazoyl-9-ylphenyl)amine (TCTA) as donor and 4,6-bis(3,5-di(pyridinyl)phenyl)-2-methylpyrimidine (PyMPM) isomers as acceptor have been reported to exhibit external quantum efficiencies (EQEs) of more than 25% – however, only at low temperature.[6–8] In an attempt to understand and improve TADF performance, the position of the pyridyl nitrogen has been altered, which influences the electronic structure, the dipole moment, as well as the exciplex geometry and the thin film morphology of these isomers.[9,10] However, it is difficult to gain direct insight into the exact exciplex structure and its orientation in the bulk, because the complexes will be randomly oriented in a largely amorphous film of co-deposited donor and acceptor molecules.[11] Understanding the influence of isomerism on the complex geometry and its performance would greatly support the development of new, potent exciplex TADF emitters for application in electroluminescent devices. Unfortunately, the peripheral di(pyridinyl)phenyl units of PyMPMs limit structural versatility to *ortho*-, *meta*- and *para*-orientation of the pyridinyl-*N*.[12] Asymmetric isomers, where the *N*-position is further permutated, are synthetically challenging and have not been achieved in PyMPMs. By contrast, structurally related bis(terpyridine) pyrimidines (BTPs), enable this freedom in design and allow synthesis of asymmetric *N*-isomers for fine-tuning of the dipole moments of these BTP acceptor molecules.[13–16] However, only some of the possible asymmetric BTP isomers have been reported to date and none of them have been employed in exciplexes or as TADF emitters.[15–19]

In this work, we first report the synthesis of two unprecedented asymmetric BTPs and investigate the influence of regioisomerism on the luminescence properties of TCTA:BTP exciplexes. In a second step, we resolve the lowest energy orientation of the best performing **3,4'-BTP** isomer in the

[a] *Institute of Organic and Macromolecular Chemistry, Ulm University, Albert-Einstein-Allee 11, 89081 Ulm, Germany. E-mail: alexander.kuehne@uni-ulm.de, ulrich.ziener@uni-ulm.de*
[b] *SUPA, School of Physics and Astronomy, University of St Andrews, North Haugh, St Andrews, Fife KY16 9SS, UK. E-mail: mcq6@st-andrews.ac.uk*
[c] *Humboldt Centre for Nano- and Biophotonics, Department of Chemistry, University of Cologne, Greinstraße 4-6, 50939 Köln, Germany.*
[d] *Institute of Physical Chemistry, RWTH Aachen University, Melatener Str. 20, 52074 Aachen, Germany.*
[e] *Institute of Theoretical Chemistry, Ulm University, Albert-Einstein-Allee 11, 89081 Germany.*
[f] *Helmholtz Institute Ulm Electrochemical Energy Storage (HIU), Helmholtzstraße 11, 89081 Ulm, Germany.*
[g] *DWI – Leibniz-Institute for Interactive Materials, Forckenbeckstraße 50, 52074 Aachen, Germany.*
Electronic Supplementary Information (ESI) available: Experimental details alongside with an extended discussion of the STM investigation are provided. See DOI: 10.1039/x0xx00000x

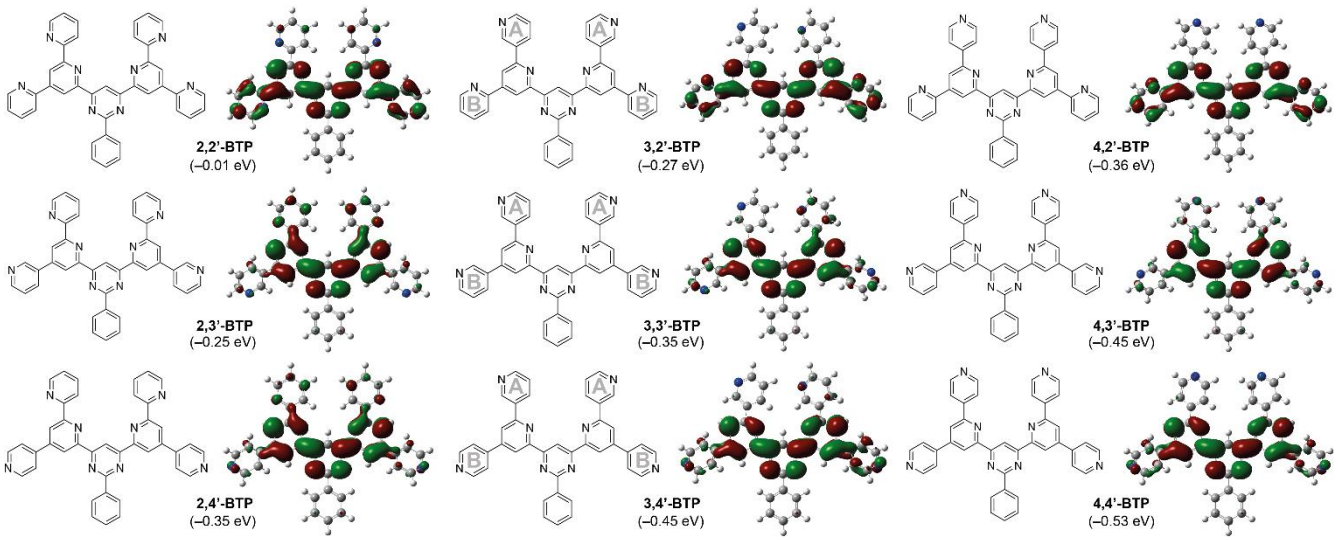

Figure 1 | Chemical structures of the nine BTP isomers that are obtained through regioisomerism in the peripheral pyridine rings, and illustration of the SOMO distributions simulated for the case of BTP radical anions. The SOMOs are calculated at the B3LYP/6-311+G(d) level.

respective complex using scanning tunneling microscopy (STM) alongside with density functional theory (DFT) and force-field simulations. Finally, we correlate the influence of regioisomerism in TCTA:BTP with their electroluminescence efficiency in OLEDs.

Results and discussion

Simulation of regioisomerism effects on the BTP acceptor properties

To determine the electronic differences between different BTP isomers and to identify the most promising structures, we first model all possible nine BTP *N*-isomers. To imitate the electronic exciplex state of the electron accepting BTP isomers after electron transfer from a donor molecule, we treat the BTPs as radical anions. First, we identify the lowest energy ground state conformer on the semi-empirical GFN2-xTB level[20,21] and reoptimize using the DFT method PBEh-3c.[22] Then we simulate the single occupied molecular orbitals (SOMOs) of the different radical anion isomers using DFT (B3LYP/6-311+G(d)). In all isomers, the additional electron resides mainly on the pyrimidine-core of the molecule as well as on the neighboring lateral pyridines (B-rings) (see Figure 1). In most cases, the A-rings of the terpyridine units do not participate significantly in the SOMO (see Figure 1). Consequently, variation of the *N*-position in the A-ring only slightly affects the SOMO. By contrast, regioisomerism in the B-rings induces a change in the extension of the SOMO accompanied by a change of its energy (see Figure 1). Greater extension of the SOMO from **3,4'-BTP** to **3,2'-BTP** leads to a reduction in the orbital energy. Due to the stronger effect of regioisomerism in the B-rings compared to the A-rings, we focus our investigation on exciplexes of the **3,2'-BTP**, **3,3'-BTP**, and **3,4'-BTP** column. Synthetic access to the asymmetric **3,2'-BTP** and **3,4'-BTP** has not been reported to date.

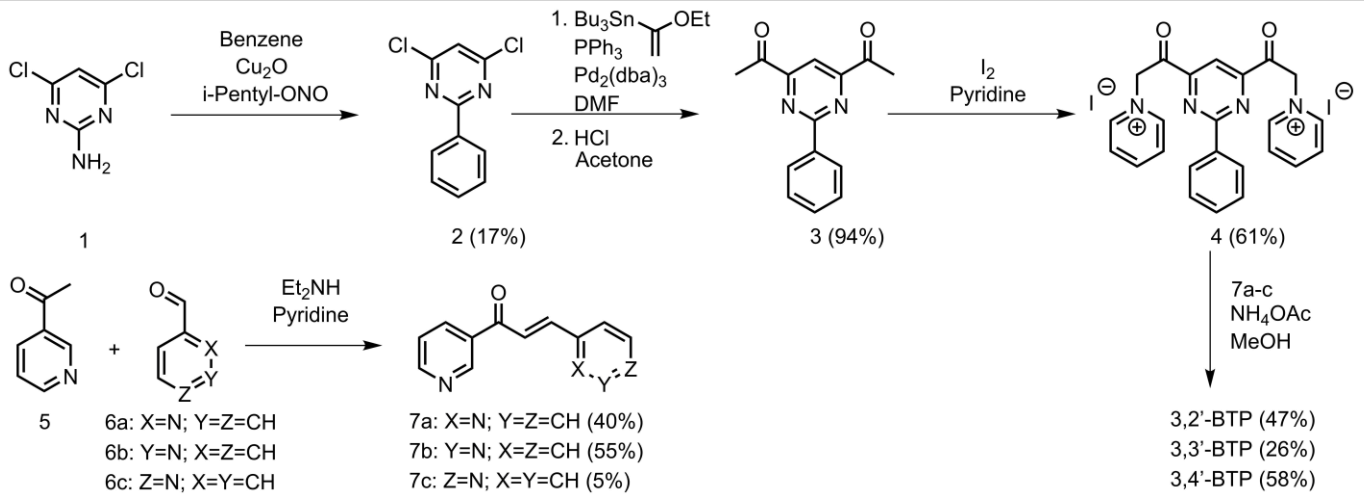

Figure 2 | Synthetic route for the three BTP isomers **3,2'-BTP**, **3,3'-BTP**, and **3,4'-BTP**. Reaction yields are stated in parentheses. Detailed reaction procedures are provided in the Supplementary Information.

Table 1 | Physical properties of the TCTA donor and the individual BTP acceptors.

	IP[a)] [eV]	EA[a)] [eV]	E_g[a)] [eV]	$E_{S_0 \rightarrow S_1}$[b)] [eV]	IP[c)] [eV]	EA[e)] [eV]	E_g[f)] [eV]	E_{HOMO}[c)] [eV]	E_{HOMO}[g)] [eV]	T_{dec}[h)] [°C]
3,2'-BTP	7.6	1.2	6.5	4.3	6.7	3.3	3.4	6.0	-5.91	498
3,3'-BTP	7.8	1.3	6.5	4.3	6.8	3.4	3.4	6.2	-6,02	492
3,4'-BTP	7.9	1.4	6.5	4.3	7.0	3.6	3.4	6.3	-6.07	501
TCTA	6.4	0.3	6.1	4.2	5.82[d)]	2.14[d)]	3.68[e)]	-	-5.72[i)]	

[a)]Computed vertically at the PBE0/def2-TZVP level on the PBEh-3c S_0 geometry.[22,45,46] [b)]Computed for the neutral system at the TDA-PBEh-3c//PBEh-3c level. [c)]Determined via UPS. E_{HOMO} with respect to Fermi energy. $IP = E_{HOMO\text{-}onset} + \Phi$. [d)]Taken from reference [47]. [e)]Calculated using $EA = IP - E_g$. [f)]Determined as the absorption onset of the normalized UV-vis spectra. [g)]Determined by cyclic voltammetry in accordance with reference [48] $E_{HOMO} = -(E_{Ox\text{-}onset/Fc} + 5.39)$ eV. [h)]Determined using TGA. [i)]Taken from reference [38].

Synthesis of BTP regioisomers

Generally, BTPs are accessible *via* the Kroehnke ring-closing reaction.[15,23,24] The required diazachalcones (**7a-c**) are prepared *via* the Claisen-Schmidt condensation between 3-acetylpyridine (**5**) and the different isomers of pyridylcarbaldehyde (**6a-c**).[25,26] In a variation of the literature protocol[17] **3,3'-BTP** is obtained by coupling **7b** to the pyrimidine diketone precursor **3**. For the first time, we have produced **3,2'-BTP** and **3,4'-BTP,** which are only accessible *via* the pyridinium salt **4** (see Figure 2). Despite the different synthetic routes, all three BTP isomers readily precipitate from their reaction solutions in high purity. For evaporation of thin films we purify the BTPs by sublimation (see Experimental in the Supplementary Information for further details).

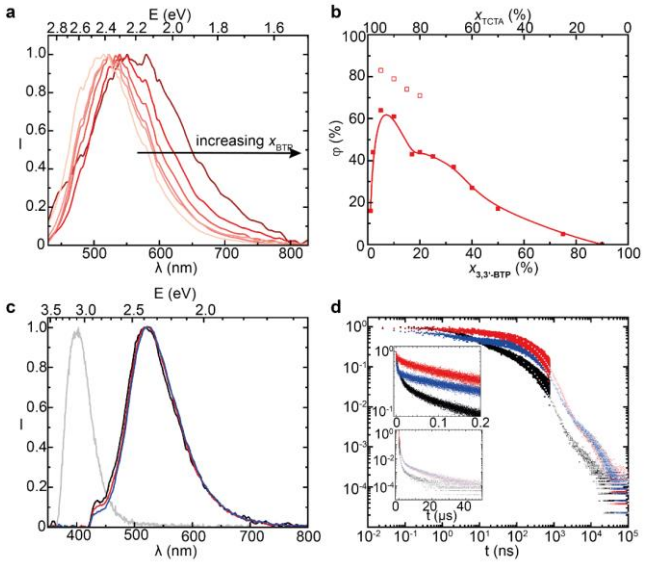

Figure 3 | a) Photoluminescence spectra of drop-cast TCTA:**3,3'-BTP** exciplex films reveal a shift toward lower energy exciplexes with increasing mole fraction of **3,3'-BTP** x_{BTP} (displayed as a gradient from light red to dark red: 1%, 10%, 25%, 50%, 75%, and 90% BTP, respectively). b) Photoluminescence quantum yield versus TCTA:**3,3'-BTP** mole fraction *x*, of drop-cast (full squares) and evaporated (open squares) films; the line is a guide to the eye. c) Photoluminescence spectra of vapor-deposited films of TCTA (grey) and the different TCTA:BTP 10:1 exciplexes (**3,2'-BTP** in black; **3,3'-BTP** in red; **3,4'-BTP** in blue). d) Transient photoluminescent spectroscopy of the TCTA:BTP exciplex films (**3,2'-BTP** in black; **3,3'-BTP** in red; **3,4'-BTP** in blue). Solid data points are recorded by TCSPC, empty data point using a ns-pulsed laser and a fast CCD camera. The combined decay profiles reveal three decay regimes; the insets display single logarithmic plots of the short- and long-term components.

Exciplex formation and its photoluminescence

The synthesized BTPs alone show no fluorescence in thin films and only weak fluorescence in solution. However, when we co-deposit **3,3'-BTP** together with TCTA, we observe fluorescence that spectrally shifts with the ratio of TCTA to BTP. This occurrence of fluorescence indicates the formation of exciplexes, where the TCTA represents the donor and the different BTPs represent the acceptor moieties. We determine the physical properties of the individual components using DFT, cyclic voltammetry, as well as using ultraviolet photoelectron spectroscopy (UPS) (see Figure S1). The evaporated films of pure BTPs are free of holes and flat (see Figure S2). X-ray photoelectron spectroscopy (XPS) performed alongside UPS on all three BTPs shows C and N as the only elements, with two C 1s peaks and one N 1s peak at around 285.1 (C_1), 286,0 (C_2) and 399.1 eV, respectively, characteristic for C-C and C-N binding in aromatic molecules. Furthermore, XPS gives constant ratios between the two components in the C 1s range of $C_1 : C_2$ of 25 : 15 as well as C to N ratios of around 5, (within the limits of accuracy), all of which corroborate that the desired BTP compounds ($C_{40}H_{26}N_8$) have been synthesized. The corresponding UPS measurements reveal the HOMO energies and work functions for all BTPs (cf. Figure S1 and Table 1).

The electron affinities (*EA*) of the accepting BTPs increase from the 3.2'- to the 3,4'-isomer. This is true for both calculated and measured values. The ionization potentials (*IP*) display the same trend leading to overall comparable gaps E_g (see Table 1). The requirement for exciplex formation is met by the fact that *IP* and *EA* are higher for the BTP acceptor than for the TCTA donor, allowing efficient charge transfer. The computed and measured values correlate well with *IP* and *EA* data reported for the structurally related PyMPMs.[8]

The fluorescence maximum (λ_{max}) of TCTA alone is at 403 nm, whereas the newly observed signal for co-deposited films shifts from λ_{max} = 514 to 580 nm with increasing BTP content (see Figure 3a). This observation indicates the presence of exciplexes with different energies, due to varying alignment between donor and acceptor, which is typical for exciplexes. On the one

Table 2 | Summary of the key characteristics of TCTA:3,N'-BTP (10:1) exciplex films.

	λ_{max} [nm/eV]	Φ_{dc} (N_2/air) [%]	ϕ_{evap} (N_2) [%]	τ_1 [ns]	τ_2 [ns]	τ_3 [µs]	ϕ_1 [a] [%]	ϕ_2 [a] [%]	ϕ_3 [a] [%]	^{1}CT [b] [nm/eV]	^{3}CT [b] [nm/eV]	^3LE_a [b] [nm/eV]	^3LE_d [b] [nm/eV]	a	EQE_{max} [c] [%]
TCTA:**3,2'-BTP**	518/2.39	29/27	70	9	350	11	3.4	22	3.4	515/2.41	520/2.39	408/3.04	405/3.06	0.362	0.51
TCTA:**3,3'-BTP**	524/2.37	34/33	79	2	430	12	0.6	25	8.3	521/2.38	524/2.36	408/3.04	399/3.10	0.412	0.64
TCTA:**3,4'-BTP**	526/2.36	49/46	74	4	460	12	0.5	42	6.1	525/2.36	527/2.35	407/3.05	402/3.08	0.385	1.97

a) Determined from transient photoluminescence experiments according to reference [28]. b) Calculated at the Tamm-Dancoff approximated PBEh-3c level for the lowest energy exciplex at the S_1 geometry *in vacuo*. The states were identified via visual inspection of the natural transition orbitals. c) Determined from OLED stacks as described in the Supplementary Information.

hand, at larger amounts of TCTA, mainly high-energy exciplexes are formed. On the other hand, at high BTP content, low energy exciplexes are observed preferably.[27]

To find a suitable ratio of BTP in TCTA, we first study the photoluminescence quantum yield (ϕ_{dc}) of drop-cast films and observe and increase for higher TCTA fractions before ϕ collapses above ~95% of TCTA (see Figure 3b). This trend corresponds well with evaporated films of different TCTA:BTP ratios. However, we observe increased ϕ_{evap} compared to the drop-cast films, probably due to a higher yield in formation of TCTA:BTP complexes (see Figure 3b). To make use of the high ϕ_{evap}, we prepare films of exciplexes by vapor deposition, with evaporation ratios of 10:1 of TCTA to **3,2'-BTP**, **3,3'-BTP**, and **3,4'-BTP**, respectively (the decomposition of the BTPs occurs only around T_{dec} = 500 °C, determined by thermogravimetric analysis (TGA), see Table 1). The different exciplexes show almost identical emission spectra with maxima around 520 nm (see Figure 3c). By contrast, ϕ_{evap} varies between 70% for the TCTA:**3,2'-BTP** exciplex and 79% for the TCTA:**3,4'-BTP** exciplex (see Table 2). All TCTA:BTP exciplex films exhibit improved ϕ_{dc} by about 2% in nitrogen compared to air, indicating that triplet states are quenched by oxygen. TADF and reverse intersystem crossing (RISC) from triplet to emissive singlet states may take place under inert atmosphere (see Table 2). To examine exciton conversion further, we record transient photoluminescence spectra of thin films of our complexes. We observe that all three exciplexes show three components to their lifetime decay: A first component of the order of a few nanoseconds, a second ranging from 350 to 460 ns and a third between 11 and 12 µs (see Figure 3d and Table 2). This multiexponential decay is in agreement with the predicted mechanism for exciplex luminescence.[28] We attribute the first component to prompt fluorescence from the charge transfer singlet state (^{1}CT). The second component results from delayed fluorescence after RISC from a locally excited triplet state (^{3}LE) to the ^{1}CT. While **3,3'-BTP** and **3,4'-BTP** exhibit strong second components, **3,2'-BTP** displays the smallest contribution of delayed fluorescence (see Figure 3d and Table 2).[29] The emission of the third component is red-shifted compared to the emission of the shorter components (see Figure S5). The long lifetime and red-shifted emission might indicate that this long component corresponds to room-temperature phosphorescence from the charge transfer triplet state (^{3}CT).

Next, we use angle-resolved photoluminescence spectroscopy to investigate the average dipole orientation of TCTA:BTP exciplexes (10:1) in vapor-deposited films. For all three exciplexes the order parameter a is > 0.33, indicating a preferred vertical dipole orientation within the films (see Table 2 and Figure S6). BTP molecules in thin films have been reported to be oriented horizontally due to intermolecular hydrogen bonding between the BTP units, causing them in the most extreme cases to assemble into two-dimensional sheets.[17] For exciplex emitters, such a horizontal orientation of the BTP units leads to a perpendicular and thus vertical orientation of the dipole moment of the exciplex. Although this vertical dipole orientation leads to reduced light out-coupling performance,[30] in PyMPMs it has been shown to improve charge transport normal to the aligned π-system.[8,31]

Exciplex structure

To better understand the influence of isomerism on the exciplex geometry, we simulate the TCTA:BTP complexes for each of the selected isomers. First, we individually optimize the BTP and TCTA structures, then dock the resulting conformers of BTP and TCTA using an intermolecular force-field potential before optimizing the assembled complex structure on the PBEh-3c level (see Figure 4a,b, Figures S7-S9, and Supporting Information for details on the calculations).[32] The TCTA aligns congruently with the π-system of the BTPs (see Figures 4b and S7-S9). We also set out to image an assembled complex using STM. For this, we consecutively coat a highly oriented pyrolytic graphite (HOPG) substrate with solutions of first **3,4'-BTP** and then TCTA (both in 1,2,4-trichlorobenzene, TCB), and investigate the surface via liquid state STM. For comparison, we also image substrates coated with pure solutions of **3,4'-BTP** and TCTA. While **3,4'-BTP** delivers a periodic structure, which is typical for BTPs, TCTA does not assemble into an ordered monolayer (see Figure 4c). The mixed TCTA:**3,4'-BTP** sample produces periodic patterns, which differ from pure **3,4'-BTP** domains and reveal a conspicuous crescent shape (see Figure 4 d-f). However, atomic resolution of the features cannot be obtained, indicating incomplete thermalization at room temperature and residual mobility in the formed structures. To investigate whether the observed pattern of the STM images can be reproduced computationally, we also model STM images by sampling TCTA:**3,4'-BTP** complexes adsorbed to a graphene surface using molecular dynamics simulations based on a generalized force field.[33] By computing STM images via GFN2-xTB[34] on 100 structures sampled equidistantly in time, followed

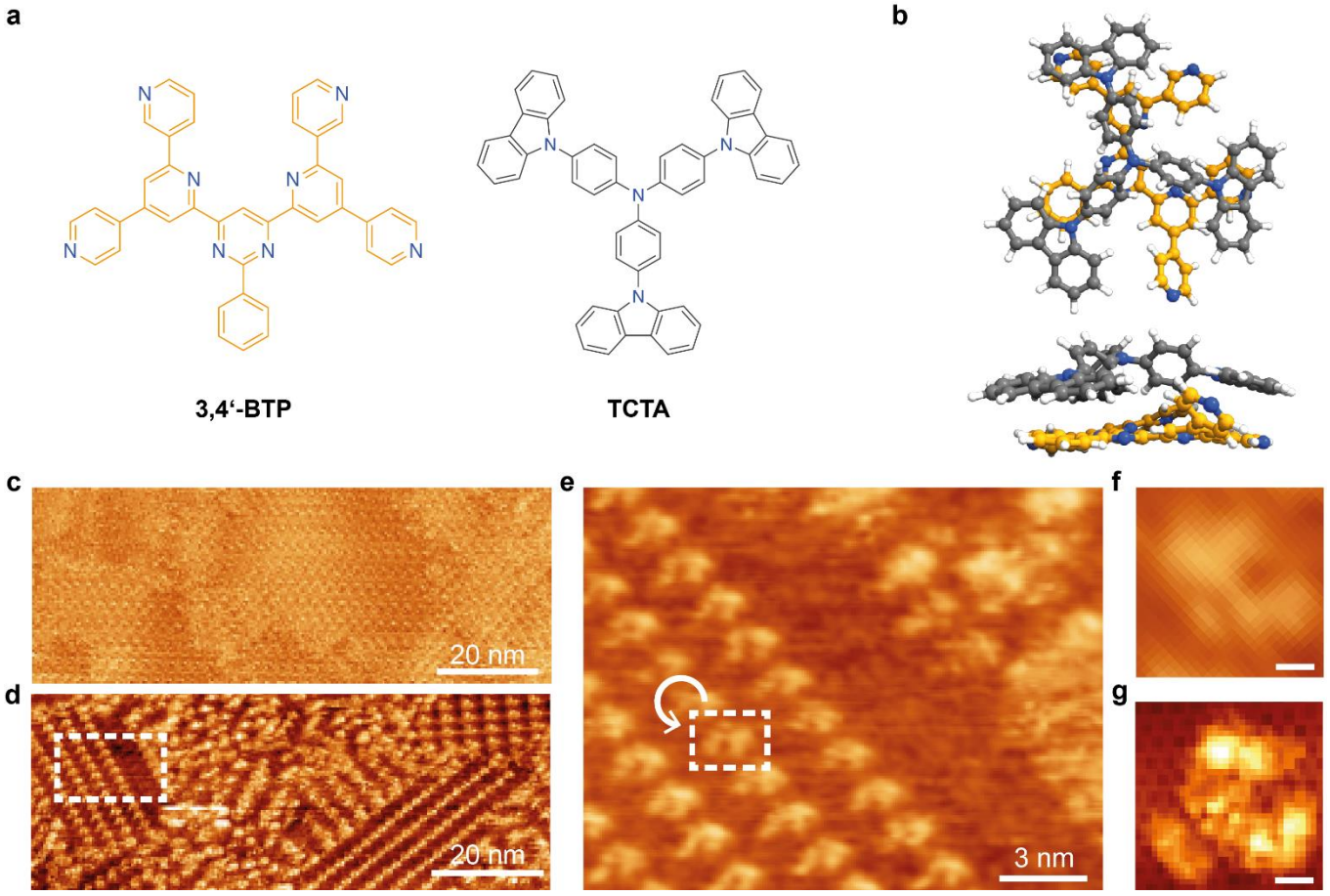

Figure 4 | a) Chemical structures of **3,4'-BTP** and TCTA. b) Top and side view of the DFT-simulated (PBEh-3c) TCTA:**3,4'-BTP** exciplex structure, with BTP coloured in orange and TCTA in grey. c, d) STM image of **3,4'-BTP** in TCB on HOPG (c) before and (d) after addition of TCTA solution. e) Close-up on the TCTA:**3,4'-BTP** exciplex structure as indicated by the white dashed box in (d). f) Zoom-in on the molecule indicated by the box in (e). The arrow indicated the direction, by which the structure has been rotated from (e) to (f) for better comparison with the modelled STM image. g) Modelled STM image of the TCTA:**3,4'-BTP** exciplex based on the 100 geometries sampled from a force-field molecular dynamics simulation on a graphene sheet (see supporting information). The scale bars in (f) and (g) represent 0.5 nm.

by superimposing and averaging, we obtain the image in Figure 4g (see Supporting Information for details). Comparison of the experimental and the modelled STM images reveals good agreement, confirming that the modelled adsorbed complex geometries resemble those exciplexes in the monolayers observed by STM (see Figure 4f,g). The crescent appearance in the STM images arises from the alignment of the carbazole units of TCTA over the terpyridine units of **3,4'-BTP**, as observed in the molecular simulations (see Figures 4b and S7-9). However, we notice some differences between the gas-phase and adsorbed geometries. Different from the gas-phase complex, the remaining carbazole of TCTA interacts less with the remaining phenyl unit of **3,4'-BTP** (see Figure 4 and Supporting Information for further details). In the adsorbed structure, the carbazole is shifted into the gap next to the phenyl group favorably interacting with the graphene sheet. We hypothesize that such complex geometries will also form in thin films co-assembled from the BTP and TCTA compounds.

Based on the gas-phase DFT-optimized complex geometries, we calculate the energy levels of the emissive ^{1}CT states and all states that are energetically close to them. These states are ^{1}CT and ^{3}CT states, originating from the exciplex of TCTA and BTP as well as the respective LE triplet states on the acceptor (^3LE_a) and the donor (^3LE_d) molecules. The excited state energy levels are determined within the Tamm-Dancoff approximation at the PBEh-3c level (see Figure 5). [22,35–37]

We find the lowest ^{1}CT state of each system to be around 2.4 eV. These results are in reasonable agreement with the experimentally determined fluorescence onset of each system corresponding to energies of 2.66 – 2.68 eV (see Figure 3 and Table 2). The ^3LE_d state is of around 3 eV. The ^3LE_a states are situated slightly below the ^3LE_d states, showing only little influence of the BTP isomerism. By contrast, the ^{3}LE energy of pure TCTA, with a phosphorescence onset at 436 nm corresponds to a much lower energy of 2.84 eV, determined at -196 °C (see Figure S24).[38] The respective phosphorescence onsets of the BTPs determined at -196 °C are between 420 and 425 nm or 2.95 and 2.92 eV (see Figure S24). The energy gap between the ^{3}LE states and the lowest-energy ^{1}CT state is relatively large (≈ 0.5 eV); however, stable hot triplet states are typically seen for triplet energy gaps of ≈ 1.0 eV. In conventional type III TADF systems the interplay of LE and CT states is crucial for RISC, and the localization of LE together with CT states seems to point towards RISC among these hot excited states (see Figure 5). However, especially in exciplex TADF systems, there is a plethora of degrees of rotational, vibrational and translational freedom, which will influence the energy of the LE states and might give more weight to the triplet states of the individual TCTA and BTP components, which would entail RISC from charge transfer T_1 to S_1, even in the

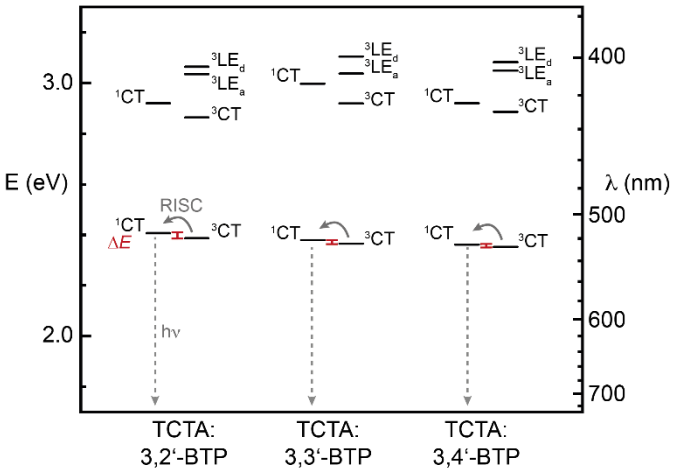

Figure 5 | Energy schemes and possible relaxation mechanism of the TCTA:**3,2'-BTP**, TCTA:**3,3'-BTP**, and TCTA:**3,4'-BTP** exciplexes in the S_1-geometry, respectively. Triplet states shown on the right, and singlet states on the left. Energies of the individual donor and acceptor molecules in red.

absence of close-by LE states in the exciplex geometry (see Table 2 and Figure 5).[39] Under such conditions, RISC is facilitated for example via hyperfine coupling between close lying T_1 and S_1 states or through the above described degrees of freedom.[40,41] The larger T_1-S_1 energy gap in **3,2'-BTP** compared to **3,3'-BTP** and **3,4'-BTP** would suggest that **3,2'-BTP** will form the least well performing TADF exciplex in the series. We therefore conclude that RISC will preferentially occur from T_1 to S_1 as the major pathway; however, depending on the exciplex geometry, there might also be RISC among higher level CT and LE states resembles hot exciton and hot exciplex TADF processes.[42–44] The fact that the lowest-energy 1CT states of our three isomers are nearly isoenergetic agrees well with their nearly indistinguishable photoluminescence spectra (see Figure 3c). By contrast, the TADF process will be different in the isomers, as already indicated by the differences observed in the transient photoluminescence measurements (see Figure 3d).

Electroluminescence of TCTA:BTP exciplexes

Finally, we investigate whether the different values of ϕ and a translate to differences in the performance of OLEDs made from the respective BTP isomers. As films with excess TCTA show superior ϕ compared to 1:1 exciplexes, we fabricate OLEDs with TCTA:BTP ratios of 10:1. The OLED stacks have the following composition and layer thickness: ITO/ TAPC (60 nm)/ TCTA (10 nm)/ TCTA:BTP (10:1, 30 nm)/ BTP (30 nm)/ LiF (1 nm)/ Al (100 nm) (see Figure 6a). The corresponding electroluminescence spectra agree well with the photoluminescence spectra of 10:1 TCTA:BTP films, indicating that the same exciplex species are responsible for emission (cf. Figure 3c and Figure 6b). By contrast, the EQEs differ considerably between 0.5 and ca. 2.0% for the different BTP isomers (see Table 2 and Supporting Information). As expected from the DFT calculation above, 3,2'-BTP is the least performant with regards to TADF.

The EQE of an OLED is the product of the electric efficiency γ, the radiative exciton production efficiency η_r, ϕ_{evap}, and the light outcoupling efficiency η_{OC}:

$$EQE = \gamma \cdot \phi_{evap} \cdot \eta_r \cdot \eta_{oc}. \quad (1)$$

While ϕ_{evap} varies for the different exciplexes of BTP isomers, this factor explains only part of the observed EQE difference. γ is expected to be similar for all BTPs. To estimate the lower limit of TADF contribution to the emission, we assume η_{OC} = 0.2, which is typical for isotropic dipole orientation of the emitter. In doing so, we slightly underestimate the performance of our devices as our materials show an orientation factor a in line with moderate vertical dipole orientation. If we assume further that the least well performing **3,2'-BTP,** has negligible TADF contribution to the overall emission, i.e. η_r = 0.25, we can assume γ = 0.15 to calculate the lower limit for the exciton production efficiencies η_r from equation (1) . These are 28% for **3,3'-BTP** and 91% for **3,4'-BTP**. This conservative approximation implies that efficient TADF is taking place in these device.

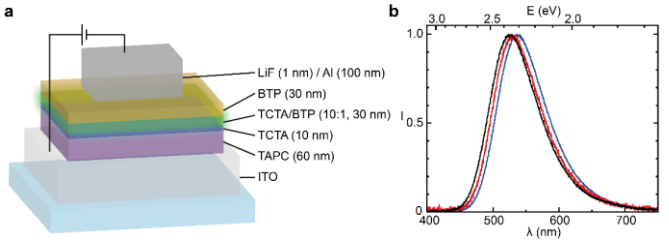

Figure 6 | a) Architecture of the fabricated OLEDs. b) Electroluminescence spectra of the TCTA:**3,2'-BTP** (black), TCTA:**3,3'-BTP** (red), and TCTA:**3,4'-BTP** (blue) exciplexes.

Conclusions

In summary, we introduce BTPs as suitable acceptor units in exciplexes and discuss the influence of isomerism on the TADF performance of the exciplex emission. The combination of STM with DFT enables precise structure elucidation and validation of the quantum mechanical calculations of the electronic states. Even beyond the field of TADF emitter materials, this technique will provide a powerful tool for correlating supramolecular 2D structures with the electronic properties of organic materials – and *vice versa.*

Author Contributions

The project was devised by AJCK. Synthesis of the BTPs was carried out by ALS. Optical properties of the exciplexes were investigated by ALS, FDG, MCG, SH, AM and FTC. Quantum-chemical simulations were performed by CB and ALS. FB performed UPS analysis. MU, PJW and FDG performed cyclic voltammetry, AFM and spectroscopic analysis. Devices were fabricated and characterized by MCG, SH, and SK. STM experiments were performed and evaluated by UZ. ALS and AJCK wrote the first draft. All authors evaluated the data and contributed to writing the manuscript.

Conflicts of interest

There are no conflicts to declare.

Acknowledgements

We thank Daniel Perleth and Maximilian Philipp (both at Ulm University) for their support during synthesis. A.L.S. acknowledges financial support through a Cusanuswerk scholarship. The authors acknowledge support by the state of Baden-Württemberg through bwHPC and the German Research Foundation (DFG) through grant no INST 40/575-1 FUGG (JUSTUS and JUSTUS 2 cluster). M.C.G. acknowledges support from the Leverhulme Trust (RPG-2016047) and the Alexander von Humboldt Stiftung through the Humboldt-Professorship. A.M. acknowledges support from the European Union's Horizon 2020 research and innovation programme under the Marie Skłodowska-Curie grant agreement No. 101023743 (PolDev). C.B. acknowledges funding by the BMBF and the Ministry of Culture and Science of the German State of North Rhine-Westphalia (MKW) under the Excellence Strategy of the Federal Government and the Länder. Simulations were performed with computing resources granted by RWTH Aachen University under project rwth0713.

Notes and references

(1) Hirata, S.; Sakai, Y.; Masui, K.; Tanaka, H.; Lee, S. Y.; Nomura, H.; Nakamura, N.; Yasumatsu, M.; Nakanotani, H.; Zhang, Q.; et al. Highly Efficient Blue Electroluminescence Based on Thermally Activated Delayed Fluorescence. *Nat. Mater.* **2015**, *14*, 330–336.

(2) Chen, X.-K.; Kim, D.; Brédas, J.-L. Thermally Activated Delayed Fluorescence (TADF) Path toward Efficient Electroluminescence in Purely Organic Materials: Molecular Level Insight. *Acc. Chem. Res.* **2018**, *51*, 2215–2224.

(3) Cai, X.; Su, S.-J. Marching Toward Highly Efficient, Pure-Blue, and Stable Thermally Activated Delayed Fluorescent Organic Light-Emitting Diodes. *Adv. Funct. Mater.* **2018**, *28*, 1802558.

(4) Liang, X.; Tu, Z.-L.; Zheng, Y.-X. Thermally Activated Delayed Fluorescence Materials: Towards Realization of High Efficiency through Strategic Small Molecular Design. *Chem. – A Eur. J.* **2019**, *25*, 5623–5642.

(5) Sarma, M.; Wong, K. T. Exciplex: An Intermolecular Charge-Transfer Approach for TADF. *ACS Appl. Mater. Interfaces* **2018**, *10*, 19279–19304.

(6) Kim, K.-H.; Yoo, S.-J.; Kim, J.-J. Boosting Triplet Harvest by Reducing Nonradiative Transition of Exciplex toward Fluorescent Organic Light-Emitting Diodes with 100% Internal Quantum Efficiency. *Chem. Mater.* **2016**, *28*, 1936–1941.

(7) Park, Y.-S.; Kim, K.-H.; Kim, J.-J. Efficient Triplet Harvesting by Fluorescent Molecules through Exciplexes for High Efficiency Organic Light-Emitting Diodes. *Appl. Phys. Lett.* **2013**, *102*, 153306.

(8) Sasabe, H.; Tanaka, D.; Yokoyama, D.; Chiba, T.; Pu, Y.-J.; Nakayama, K.; Yokoyama, M.; Kido, J. Influence of Substituted Pyridine Rings on Physical Properties and Electron Mobilities of 2-Methylpyrimidine Skeleton-Based Electron Transporters. *Adv. Funct. Mater.* **2011**, *21*, 336–342.

(9) Gather, M. C.; Reineke, S. Recent Advances in Light Outcoupling from White Organic Light-Emitting Diodes. *J. Photonics Energy* **2015**, *5*, 057607.

(10) Brütting, W.; Frischeisen, J.; Schmidt, T. D.; Scholz, B. J.; Mayr, C. Device Efficiency of Organic Light-Emitting Diodes: Progress by Improved Light Outcoupling. *Phys. status solidi* **2013**, *210*, 44–65.

(11) Lin, T.-C.; Sarma, M.; Chen, Y.-T.; Liu, S.-H.; Lin, K.-T.; Chiang, P.-Y.; Chuang, W.-T.; Liu, Y.-C.; Hsu, H.-F.; Hung, W.-Y.; et al. Probe Exciplex Structure of Highly Efficient Thermally Activated Delayed Fluorescence Organic Light Emitting Diodes. *Nat. Commun.* **2018**, *9*, 3111.

(12) Hung, W.-Y.; Chiang, P.-Y.; Lin, S.-W.; Tang, W.-C.; Chen, Y.-T.; Liu, S.-H.; Chou, P.-T.; Hung, Y.-T.; Wong, K.-T. Balance the Carrier Mobility To Achieve High Performance Exciplex OLED Using a Triazine-Based Acceptor. *ACS Appl. Mater. Interfaces* **2016**, *8*, 19.

(13) Ziener, U. Self-Assembled Nanostructures of Oligopyridine Molecules. *J. Phys. Chem. B* **2008**, *112*, 14698–14717.

(14) Goll, F. D.; Schleper, A. L.; Kuehne, A. J. C.; Ziener, U. Effect of a Bromine Substituent on the Self-Assembly of an Oligopyridine at the Liquid|Solid Interface. *J. Phys. Chem. C* **2020**, *124*, 20213–20221.

(15) Ziener, U.; Lehn, J.-M.; Mourran, A.; Möller, M. Supramolecular Assemblies of a Bis(Terpyridine) Ligand and of Its [2×2] Grid-Type ZnII and CoII Complexes on Highly Ordered Pyrolytic Graphite. *Chem. - A Eur. J.* **2002**, *8*, 951–957.

(16) Caterbow, D.; Künzel, D.; Mavros, M. G.; Groß, A.; Landfester, K.; Ziener, U. Septipyridines as Conformationally Controlled Substitutes for Inaccessible Bis(Terpyridine)-Derived Oligopyridines in Two-Dimensional Self-Assembly. *Beilstein J. Nanotechnol.* **2011**, *2*, 405–415.

(17) Meier, C.; Ziener, U.; Landfester, K.; Weihrich, P. Weak Hydrogen Bonds as a Structural Motif for Two-Dimensional Assemblies of Oligopyridines on Highly Oriented Pyrolytic Graphite: An STM Investigation. *J. Phys. Chem. B* **2005**, *109*, 21015–21027.

(18) Ruben, M.; Ziener, U.; Lehn, J.-M.; Ksenofontov, V.; Gütlich, P.; Vaughan, G. B. M. Hierarchical Self-Assembly of Supramolecular Spintronic Modules into 1D- and 2D-Architectures with Emergence of Magnetic Properties. *Chem. - A Eur. J.* **2005**, *11*, 94–100.

(19) Meier, C.; Landfester, K.; Künzel, D.; Markert, T.; Groß, A.; Ziener, U. Hierarchically Self-Assembled Host–Guest Network at the Solid–Liquid Interface for Single-Molecule Manipulation. *Angew. Chemie Int. Ed.* **2008**, *47*, 3821–3825.

(20) Pracht, P.; Bohle, F.; Grimme, S. Automated Exploration of the Low-Energy Chemical Space with Fast Quantum Chemical Methods. *Phys. Chem. Chem. Phys.* **2020**, *22*, 7169–7192.

(21) Bannwarth, C.; Ehlert, S.; Grimme, S. GFN2-XTB—An Accurate and Broadly Parametrized Self-Consistent Tight-Binding Quantum Chemical Method with Multipole Electrostatics and Density-Dependent Dispersion Contributions. *J. Chem. Theory Comput.* **2019**, *15*, 1652–1671.

(22) Grimme, S.; Brandenburg, J. G.; Bannwarth, C.; Hansen, A. Consistent Structures and Interactions by Density Functional Theory with Small Atomic Orbital Basis Sets. *J. Chem. Phys.* **2015**, *143*, 054107.

(23) Zecher, W.; Kröhnke, F. Eine Neue Synthese Substituierter Pyridine, I. Grundzüge Der Synthese. *Chem. Ber.* **1961**, *94*, 690–697.
(24) Eggers, B.; Ziener, U. Optically Functionalized Grid-Type Complexes by a Post-Assembly Strategy. *Chem. - A Eur. J.* **2018**, *24*, 14968–14973.
(25) Attia, A.; Michael, M. Azachalcones. *Pharmazie* **1982**, *37*, 551–553.
(26) Durinda, J.; Szücs, L.; Krasnec, L.; Heger, J.; Springer, V.; Kolena, J.; Keleti, J. No Title. *Acta Fac. Pharm. Bohem.* **1966**, *12*, 89–129.
(27) Moon, C.-K.; Huh, J.-S.; Kim, J.-M.; Kim, J.-J. Electronic Structure and Emission Process of Excited Charge Transfer States in Solids. *Chem. Mater* **2018**, *30*, 30.
(28) dos Santos, P. L.; Dias, F. B.; Monkman, A. P. Investigation of the Mechanisms Giving Rise to TADF in Exciplex States. *J. Phys. Chem. C* **2016**, *120*, 18259–18267.
(29) Tsuchiya, Y.; Diesing, S.; Bencheikh, F.; Wada, Y.; dos Santos, P. L.; Kaji, H.; Zysman-Colman, E.; W Samuel, I. D.; Adachi, C.; Tsuchiya, Y.; et al. Exact Solution of Kinetic Analysis for Thermally Activated Delayed Fluorescence Materials. *J. Phys. Chem. A* **2021**, *125*, 8074--8089.
(30) Tenopala-Carmona, F.; Lee, O. S.; Crovini, E.; Neferu, A. M.; Murawski, C.; Olivier, Y.; Zysman-Colman, E.; Gather, M. C. Identification of the Key Parameters for Horizontal Transition Dipole Orientation in Fluorescent and TADF Organic Light-Emitting Diodes. *Adv. Mater.* **2021**, *33*, 2100677.
(31) Yokoyama, D.; Sasabe, H.; Furukawa, Y.; Adachi, C.; Kido, J. Molecular Stacking Induced by Intermolecular C-H···N Hydrogen Bonds Leading to High Carrier Mobility in Vacuum-Deposited Organic Films. *Adv. Funct. Mater.* **2011**, *21*, 1375–1382.
(32) Grimme, S.; Bannwarth, C.; Caldeweyher, E.; Pisarek, J.; Hansen, A. A General Intermolecular Force Field Based on Tight-Binding Quantum Chemical Calculations. *J. Chem. Phys.* **2017**, *147*, 161708.
(33) Spicher, S.; Grimme, S. Robust Atomistic Modeling of Materials, Organometallic, and Biochemical Systems. *Angew. Chemie Int. Ed.* **2020**, *59*, 15665–15673.
(34) Tersoff, J.; Hamann, D. R. Theory and Application for the Scanning Tunneling Microscope. *Phys. Rev. Lett.* **1983**, *50*, 1998–2001.
(35) Hirata, S.; Head-Gordon, M. Time-Dependent Density Functional Theory within the Tamm-Dancoff Approximation. *Chem. Phys. Lett.* **1999**, *314*, 291–299.
(36) TURBOMOLE V7.5.1, a Development of University of Karlsruhe and Forschungszentrum Karlsruhe GmbH GmbH, a Development of University of Karlsruhe and Forschungszentrum Karlsruhe. 2021.
(37) Balasubramani, S. G.; Chen, G. P.; Coriani, S.; Diedenhofen, M.; Frank, M. S.; Franzke, Y. J.; Furche, F.; Grotjahn, R.; Harding, M. E.; Hättig, C.; et al. TURBOMOLE: Modular Program Suite for Ab Initio Quantum-Chemical and Condensed-Matter Simulations. *J. Chem. Phys.* **2020**, *152*, 184107.
(38) Mamada, M.; Tian, G.; Nakanotani, H.; Su, J.; Adachi, C. The Importance of Excited-State Energy Alignment for Efficient Exciplex Systems Based on a Study of Phenylpyridinato Boron Derivatives. *Angew. Chemie Int. Ed.* **2018**, *57*, 12380–12384.
(39) Gibson, J.; Monkman, A. P.; Penfold, T. J. The Importance of Vibronic Coupling for Efficient Reverse Intersystem Crossing in Thermally Activated Delayed Fluorescence Molecules. *ChemPhysChem* **2016**, 2956–2961.
(40) Chapran, M.; Pander, P.; Vasylieva, M.; Wiosna-Salyga, G.; Ulanski, J.; Dias, F. B.; Data, P. Realizing 20% External Quantum Efficiency in Electroluminescence with Efficient Thermally Activated Delayed Fluorescence from an Exciplex. *ACS Appl. Mater. Interfaces* **2019**, *11*, 13460–13471.
(41) Dos Santos, P. L.; Dias, F. B.; Monkman, A. P. Investigation of the Mechanisms Giving Rise to TADF in Exciplex States. *J. Phys. Chem. C* **2016**, *120*, 18259–18267.
(42) Liu, X.-K.; Chen, Z.; Zheng, C.-J.; Liu, C.-L.; Lee, C.-S.; Li, F.; Ou, X.-M.; Zhang, X.-H. Prediction and Design of Efficient Exciplex Emitters for High-Efficiency, Thermally Activated Delayed-Fluorescence Organic Light-Emitting Diodes. *Adv. Mater.* **2015**, *27*, 2378–2383.
(43) Xu, Y.; Xu, P.; Hu, D.; Ma, Y. Recent Progress in Hot Exciton Materials for Organic Light-Emitting Diodes. *Chem. Soc. Rev.* The Royal Society of Chemistry 2021, pp 1030–1069.
(44) Schleper, A. L.; Goushi, K.; Bannwarth, C.; Haehnle, B.; Welscher, P.; Adachi, C.; Kuehne, A. Hot Exciplexes in U-Shaped TADF Molecules with Emission from Locally Excited States. **2021**.
(45) Adamo, C.; Barone, V. Toward Reliable Density Functional Methods without Adjustable Parameters: The PBE0 Model. *J. Chem. Phys.* **1999**, *110*, 6158–6170.
(46) Weigend, F.; Ahlrichs, R. Balanced Basis Sets of Split Valence, Triple Zeta Valence and Quadruple Zeta Valence Quality for H to Rn: Design and Assessment of Accuracy. *Phys. Chem. Chem. Phys.* **2005**, *7*, 3297–3305.
(47) Meyer, J.; Kröger, M.; Hamwi, S.; Gnam, F.; Riedl, T.; Kowalsky, W.; Kahn, A. Charge Generation Layers Comprising Transition Metal-Oxide/Organic Interfaces: Electronic Structure and Charge Generation Mechanism. *Appl. Phys. Lett.* **2010**, *96*, 193302.
(48) Cardona, C. M.; Li, W.; Kaifer, A. E.; Stockdale, D.; Bazan, G. C. Electrochemical Considerations for Determining Absolute Frontier Orbital Energy Levels of Conjugated Polymers for Solar Cell Applications. *Adv. Mater.* **2011**, *23*, 2367–2371.

